Original Article

Institution of MECHANICAL ENGINEERS
Journal of AEROSPACE ENGINEERING

Proc IMechE Part G:
J Aerospace Engineering
2022, Vol. 236(5) 825–841

DOI: 10.1177/09544100211023627
journals.sagepub.com/home/pig
SAGE

Design and aerodynamic evaluation of a medium short takeoff and landing tactical transport aircraft

Pedro D Bravo-Mosquera[1], John J Vaca-Rios[1,2], Anny I Diaz-Molina[2], María A Amaya-Ospina[2] and Hernán D Cerón-Muñoz[1]

Abstract

The present article deals with the conceptual design of a new medium short takeoff and landing tactical transport aircraft, which is intended to expand the institutional capabilities of the Colombian Air Force in terms of versatility and flexibility. An original design strategy was developed during the conceptual design, combining classical methodologies and high-fidelity computational fluid dynamics (CFD) simulations. This methodology allowed the aircraft to be assessed in a single design space, based on its design requirements, mission, and applicable airworthiness standards. Once obtained a baseline concept, the aerodynamic study focused on the flow around two types of wingtip devices: tip tanks and blended winglets. These devices were designed to optimize the performance capabilities of the aircraft, while keeping simple certification procedures. Wind tunnel experiments and CFD simulations were carried out to evaluate and select the best configuration. Lift, drag, and pitching moment coefficient charts, along with vorticity contours, are presented. Results showed that blended winglets have a significant potential for improving aircraft performance without severe structural weight penalties, allowing additional payload capabilities and/or increased range and fuel savings. Finally, the optimized aircraft is compared to major competitors in order to discuss and highlight its main advantages and feasibility for future production.

Keywords

Short takeoff and landing, turboprop, winglets, tip tanks, wind tunnel

Date received: 7 August 2020; accepted: 17 May 2021

Introduction

Military air transport operations are divided into two broad groups: (i) strategic missions and (ii) tactical missions. High-performance transport aircraft are used in strategic missions to carry supplies, arms, and personnel over long distances, usually between two air bases that are not located in the same geographical area. An example of this category is the Boeing C-17 Globemaster III, which can transport modern tanks such as the M1 Abrams (70 tonnes), covering a range of about 11,000 km.[1] On the other hand, tactical transport missions are applied to regions with fewer territorial borders than those involved in strategic missions. This type of mission involves cargo launching activities, logistic support, and even skydiving activities. Turboprop aircraft such as the Lockheed C-130 Hercules are typically tactical transports. They are designed to operate on small and rustic runways or, as in the case of helicopters, even in locations without runways. In general, tactical aircraft operate at low altitudes to avoid radar detection, providing ground-to-air defense capability against missiles.[2]

According to the United Nations, both strategic and tactical military operations have become a central pillar for the preservation of the current international order.[3] Latin American countries such as Colombia, Mexico, Ecuador, and Bolivia, which have been in constant conflict due to drug trafficking, do not have an original configuration to deal with this problem, that is, these countries make use of retrofitted commuter planes. However, instead of improving the aircraft's effectiveness, such modifications created expensive, ineffective aircraft. As a result, there is an increasing trend to promote fleet renewal, with a focus

[1] Department of Aeronautical Engineering, São Carlos Engineering School, University of São Paulo, Brazil
[2] Programa de Ingeniería Aeronáutica, Fundación Universitaria los Libertadores, Colombia

Corresponding author:
Pedro D Bravo-Mosquera, São Carlos Engineering School, University of São Paulo, Área 2. Avenida João Dagnone, no 1100 - Jardim Santa Angelina, São Carlos 13563-120, São Paulo, Brazil.
Email: pdbravom@usp.br

on original defense programs in order to minimize foreign aircraft investment.

In the case of Colombia, the aeronautical sector has undergone significant changes over the last few years. Outstanding programs are being established to promote original aircraft design and manufacture.[4] However, progress on tactical transport aircraft has been affected by the high degree of complexity of the Colombian territory. For the sake of argument, Colombia's geography is divided into six distinct natural areas, each with its own distinct characteristics. One of them is the Andean region, where most of the population, wealth, and state are located. The other five regions are rural and remote areas (geographically more complex), where illegal armed groups have performed criminal activities, affecting the well-being of the population of those zones. There is also a limited access to food, housing, and medical treatment, causing higher infant mortality rates and thus lower life expectancy.[5]

Despite the fact that designing a tactical transport aircraft is a huge technological challenge for countries with a less developed industrial base, the aim of this work is to demonstrate the feasibility of such research projects by developing countries, increasing interest in both the civil and military sectors, and thus providing viable, low-cost alternatives. In this context, this work presents the conceptual design, aerodynamic evaluation, and performance optimization of a new tactical transport aircraft called SkyVultur (in memory of the Andean condor), whose design requirements are based on the needs that must be supplied for different military missions such as cargo or passenger transport, aerial refueling, firefighting, skydiving training, and takeoff on unprepared runways, among others. Furthermore, the authors recognized that other variants of the aircraft, such as commuter-style operations and medevac special missions, would have a business demand. As a result, the SkyVultur aircraft complies with both FAR part 23 and EASA CS-23.[6]

In the following sections, a descriptive methodology for the design of the proposed aircraft is presented. After a brief summary of the state of the art, the article describes the conceptual design stage, where the first concept is developed based on top-level design requirements. Subsequently, the aerodynamic study is presented, describing the respective computational fluid dynamics (CFD) tools and wind tunnel setup. In the end, the results are presented and discussed including the evolution of the design process and key geometry and performance features of the SkyVultur aircraft.

State of the art

Aircraft design engineers must look for ways to provide functionality and versatility, that is, the ability of a new aircraft to operate in a wide range of missions and sectors. In this context, this section provides a literature survey on design methodologies, optimization techniques, and new technologies used in the design of both a military transport aircraft and a 19-passenger commuter aircraft.

Embraer's experience in the commuter aircraft industry was very useful for designing the SkyVultur aircraft.[7] Many aircraft have been designed using the Embraer technology acquisition strategy, which involves definition of aircraft geometry, major structural analysis, detailed specification of all parts, flight control systems, material choice, and handling. Therefore, Embraer's approach to engineering knowledge taught us design skills and integration of systems. Other important technologies for commuter aircraft are listed in NASA SP, vol. 406.[8] Such technologies are defined as the main design drivers for commercial success and effectiveness of this aircraft category.

More recently, the University of Naples, in Italy, presented different techniques for evaluating the conceptual design of the P2012 Traveller aircraft. It is a twin-engine commuter aircraft designed by Prof. Luigi Pascale at Tecnam Aircraft Industries.[9] The authors described a fairly complete design methodology of the aircraft, performing weight estimates, constraint analysis, and more detailed aerodynamic assessments, focusing mainly on CFD simulations and wind tunnel experiments to study wing–fuselage interference and its effects on wing loading.[10,11] In addition, several aspects such as stability and control characteristics,[12,13] and also flight tests, performance, and flight certification,[14] have been reported by the entire research team. The above referenced publications provided an adequate framework for each design stage of the SkyVultur aircraft in order to optimize its performance.

Several conceptual design methodologies have been published, involving CFD simulations for aircraft configurations with similar characteristics to the SkyVultur aircraft. For example, Della Vecchia and Nicolosi[15] provided specific details about the aerodynamic design and optimization of future regional turboprop aircraft with about 90 passengers. The authors designed a wingtip device able to reduce the fuel consumption by about 4% during the entire mission profile. Lappas and Ikenaga[16] described the conceptual design and performance optimization of a tip device for a regional turboprop aircraft. The authors modeled the main wing as two panels, each one extending from the wingtip to the wing root position. The simulated optimal winglet achieved a 2.38% increase of the maximum range by reducing the total drag by 1.19%. Bravo-Mosquera et al.[17] presented the conceptual design and CFD optimization of a new prototype of agricultural aircraft. In this study, the authors optimized the aerodynamic efficiency of the AG-Nel 25 aircraft through a multi-winglet device. The results showed an increase in flight time and range by about 12% and 8.4%, respectively. Kaparos et al.,[18] Hosseini et al.,[19] and Bravo-Mosquera et al.[20] have used CFD simulations to study the flow behavior of different aircraft during conceptual design phases. In this context, specific computational aerodynamic studies have been performed on the SkyVultur aircraft, as a high-fidelity tool to validate its conceptual design, and to characterize the airflow around its aerodynamic surfaces.

Key design parameters in terms of aviation safety and certification requirements were obtained from Iwaniuk et al.[21,22] The authors reported a method to optimize two classes of aircraft, 9 seater and 19 seater. Some of the design requirements of the 19-seater aircraft have been used for this specific case since this number of passengers corresponds to the SkyVultur's passenger capacity. These findings indicated that the SkyVultur aircraft should meet specific technical and economic requirements in order to be competitive in the tactical and/or commuter transport aircraft markets.

Finally, Vouvakos et al.[23] presented one of the most relevant works used to validate the design of the SkyVultur aircraft. The authors developed linear correlations among key design parameters of turboprop and twin-engine aircraft. This database allowed a direct and rapid comparison of existing designs. Likewise, Marinus et al.[24–26] presented statistical data and design characteristics of turbo-propelled military and civil transport aircraft. These works also served as a method for validating the design of the SkyVultur aircraft, mainly during the mission description and weight estimations.

Design methodology

In this section, the step-by-step procedure for designing the SkyVultur aircraft is presented. A combination of traditional methods, such as the ones described in Refs. 27–29, along with computational simulations composed the entire design process. The roadmap of the conceptual design is presented in Figure 1. It should be noted that each module is an integral element of any conceptual-level aircraft design tool, so automated processes such as loops for optimization and exploration are internal parts of the framework.

First of all, design requirements were defined in order to orient sizing in a simplified, cheaper direction (i.e., following the airworthiness standards of the commuter category; FAR 23 or CS-23 regulation). Then, the first weight estimation was conducted, based mostly on semi-empirical relations and some early concept sketches. The next step was to estimate the power loading and wing loading using the constraint analysis. Such performance parameters were the basis for the design/selection of airfoil, wing area, and propulsion system. Specific aerodynamic studies were performed in the next design phase, where the wing, wingtips, fuselage, tails, and control surfaces were conceived and defined. The aerodynamic sizing was enhanced by static stability analysis.

Subsequently, investigations on some particular aerodynamic effects (such as the wing/wingtip interactions) have been carried out. In this context, a detailed high-fidelity aerodynamic analysis was conducted based on CFD simulations and wind tunnel tests. We evaluated the aerodynamic benefits of two alternatives of wingtip devices (tip tanks and blended winglets), as a way of enhancing the performance of the SkyVultur aircraft, since most aircraft of the same category, such as Dornier Do 228, PZL M28 Skytruck, CASA C-212 Aviocar, and Cessna 408 SkyCourier, did not integrate wingtip devices in their final layouts. Such results are presented highlighting performance improvements during the mission profile.

Finally, we compare the most important design features among aircraft of the same category, in order to verify if the SkyVultur aircraft meet the market demand.

Design requirements

Design requirements were defined based on the scope of the SkyVultur aircraft missions and the airworthiness standards applicable to aircraft of the commuter category. The certified commuter category includes propeller-driven twin-engine aircraft, with a single aisle seating

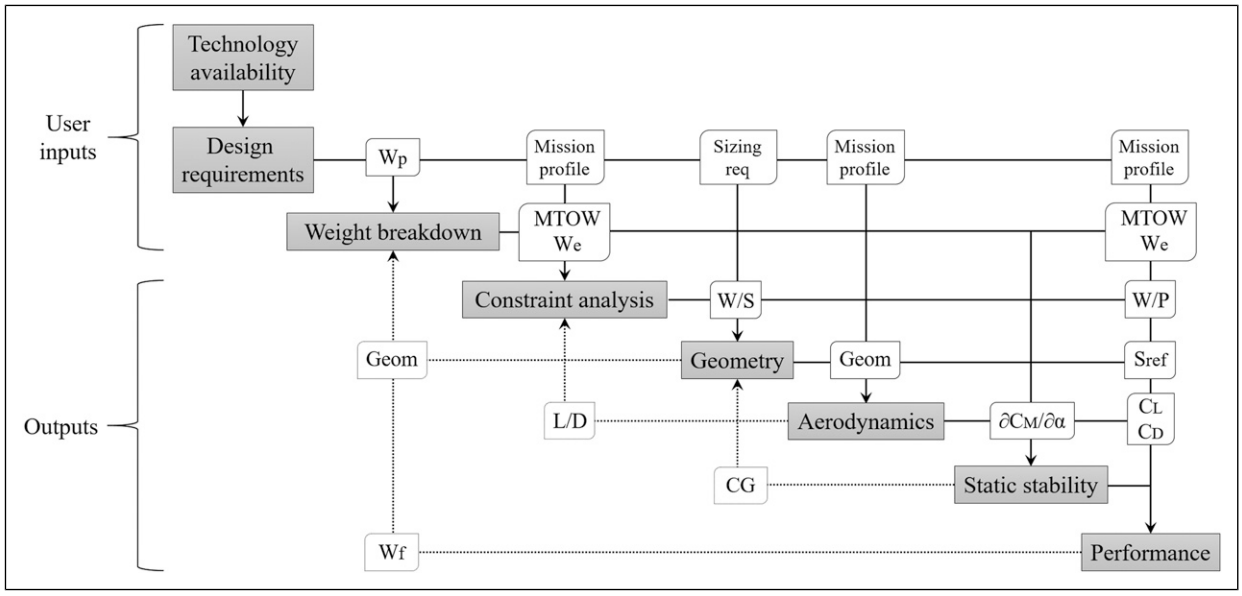

Figure 1. SkyVultur conceptual design roadmap.

configuration, a maximum of 19 seats (excluding the pilots seat), and a maximum takeoff mass of 19,000 lb (8618 kg).[6]

On the other hand, the SkyVultur aircraft missions were derived from an extensive database, which included the main features of 20 military and civil transport aircraft. Since the main objective was to define a promising concept, a parametric analysis based on the collected data was performed. We used statistical regression models and semi-empirical laws to fix the main design and mission characteristics. Thus, the database outlined several recommendations for estimating the average weight and the performance features of aircraft belonging to this group.

After analyzing the missions carried out by these aircraft (tactical transport, evacuation of injured people, firefighting, skydiving, and antidrug missions), the SkyVultur aircraft was designed following two missions (Figure 2). The first is a simple cruise mission consisting of a takeoff run (1), climb to cruise altitude (2), cruise speed to destination (3), loiter (4), descent (5), and landing (6) (see Figure 2(a)). The second is a typical skydiving and/or cargo launching mission, with a takeoff run (1), ascent to cruising altitude (2), cruising speed to the launch site (3), cargo release/paratroopers (4), second cruise (5), loiter (6), descent (7), and landing (8) (see Figure 2(b)).

Finally, considering the operation over the Colombian territory, a feasibility and trade-off analysis was conducted to assess the conditions for range and takeoff. We concluded that access to remote areas is the issue that would have the greatest impact on aircraft, not just because of geographical and meteorological conditions but also because of unprepared runways at airports. These conditions led to a set of design criteria that were grouped into two broad groups: sizing requirements and performance requirements. Table 1 presents a summary of the design requirements adopted for the SkyVultur aircraft.

Sizing requirements defined the operational needs of the aircraft. For example, a high wing provides a clear, unobstructed view of the ground as well as clearance for avoiding low obstacles, which is useful for landing on airfields with unprepared runways. Furthermore, high wings aid to reduce landing distance due to less impact of the ground effect. A T-tail configuration was imposed to avoid both propeller slipstream and wing downwash on the horizontal tail. This configuration allows the horizontal tail to provide a higher efficiency, avoiding tail vibration and buffet. The lateral and aft ramp doors were considered for fast loading and launch of equipment and/or troops. Flaps were considered to increase the wing surface during critical phases of flight, such as takeoff, landing, and approach. Finally, as the SkyVultur aircraft must operate on unprepared runways, a robust and retractable landing gear is mandatory to withstand heavy loads when impacting on the ground.

After determining the sizing and performance requirements, a first rapid rough sketch was developed. This first sketch was launched and discussed prior to begin with detailed sizing studies. The first sketch and final concept of the SkyVultur aircraft after several design loops are shown in Figure 3. Note that both configurations are somewhat similar, but the change from a full-tapered wing to a semi-tapered wing to boost short takeoff and landing (STOL) performance is a significant difference. The tail was modified from a cruciform tail to a T-tail to improve stability behavior. Four blades were first suggested to satisfy the performance criteria, but a final number of five blades were used after specific performance studies to improve thrust ranges during the mission profile. Finally, we initially proposed a tip tank to reduce induced drag and increase range and endurance; however, after aerodynamic and performance analyzes, an efficient blended winglet was assembled on the final concept. Specific details are presented hereafter.

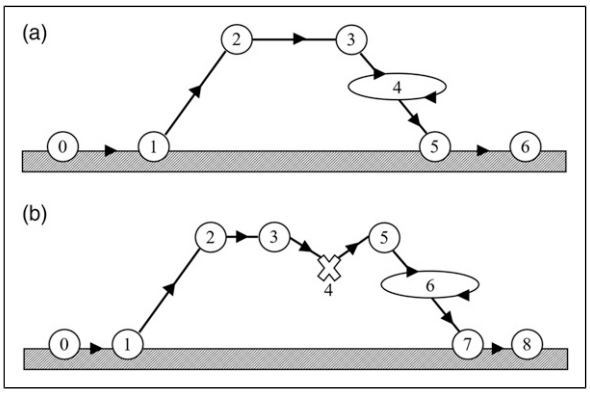

Figure 2. Mission profiles established for the SkyVultur aircraft. (a) Simple mission profile and (b) strategic mission profile.

Table 1. SkyVultur design requirements.

Sizing	Performance
High wing	Maximum cruise speed = 103 m/s
T-tail	Approach speed ≈40 m/s
Lateral door	Rate of climb ≈8.2 m/s
Aft ramp door	Takeoff distance ≈900 m
Rugged landing gear	Cargo range (full payload) = 800 km
Twin-turboprop	Service ceiling = 7600 m
No. of passengers = 19	Maximum takeoff weight ≤ 84.54 kN
No. of crew = 3	Useful payload ≈2700 kg
Flaps	—

Weight estimations

The first weight breakdown of the SkyVultur aircraft was done via its database, in which a statistical pattern was formed by linear regressions to estimate the initial maximum takeoff weight (MTOW, W_o). Subsequently, semi-empirical methods were used to break down the MTOW, in order to obtain the crew weight (W_c), empty weight (W_e), fuel weight (W_f), and payload weight (W_p).

The crew weight was derived from standardized data from the Federal Aviation Administration, indicating a weight of 80 kg for each crew member. The payload

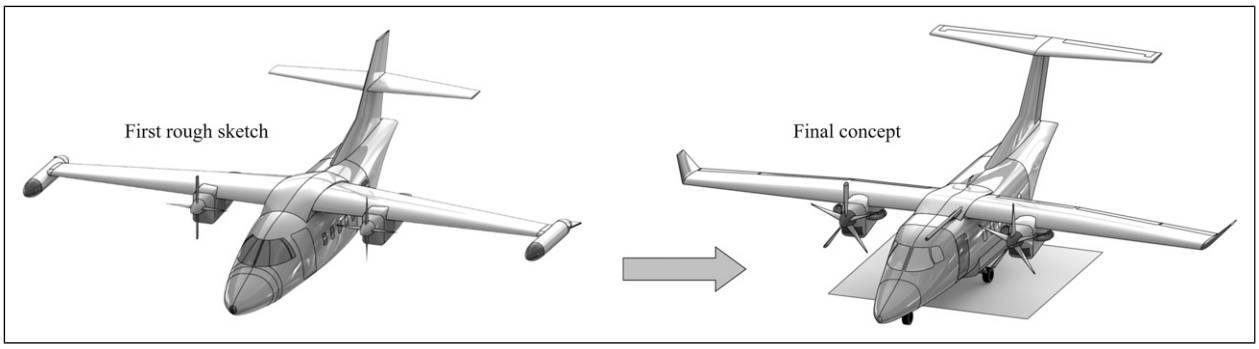

Figure 3. Initial sketch and final concept of the SkyVultur aircraft (artistic rendering).

weight was obtained directly from the design requirements, which state that the aircraft must necessarily carry a maximum number of 19 passengers. In this context, the payload weight was determined by assuming the same weight for each crew member, with a safety margin of 10 kg per passenger. In addition, it was projected that each passenger should bear 30 kg of baggage. It should be noted that the payload weight has been used for every aircraft configuration, be it cargo, parachute, or passenger. The ratio between the empty weight and the MTOW (W_e/W_o) was calculated by means of semi-empirical relations, and using aluminum alloys as manufacture material to provide considerable safety margins for the maintenance of the airframe components.[27–29] The ratio between the fuel weight and MTOW (W_f/W_o) was calculated based on the mission profiles set out in Figure 2. In this case, aerodynamic approximations were used for each flight phase, specifically with the Breguet equation. It should be noted that some flight phases, such as takeoff, climb, and descent have weight fractions that are already established in the literature.

Once identified all the aircraft weight fractions, the total fuel weight was determined assuming a reserve of 6% if the cargo is not released or skydiving activities are not performed. Therefore, an iterative process was performed until the MTOW converges to a specific value. The first calculation of the SkyVultur aircraft's weight was MTOW = 79.65 kN, W_e = 38.25 kN, W_f = 15.69 kN, and W_p varied due to the aircraft mission, having a maximum constraint of 26.48 kN. Thus, note that FAR 23 requirements were accomplished.

Constraint analysis

The constraint diagram is used to evaluate the design point at which the SkyVultur aircraft will execute the proposed mission. This analysis is extremely relevant to the aircraft, as it provides the parameters to set the wing surface and also to select the engine. Specifically, these parameters are the wing loading (W/S) and the power loading (W/P). The general equation for the constraint diagram of turboprop-powered aircraft is presented in Ref. 27. Thus, it was possible to find the solution space where the SkyVultur aircraft can perform all the design requirements such as takeoff distance (900 m, with a lift coefficient equal to 1.6), landing distance (850 m, with a lift coefficient of 1.8), rate of climb (8 m/s, with a parasite drag coefficient of 0.03), cruise speed (103 m/s), and some certification requirements such as FAR 23.65a ascent, FAR 23.65b ascent, and FAR ascent 23.77. These values have been considered reliable and achievable due to the use of high-lift devices (flaps).

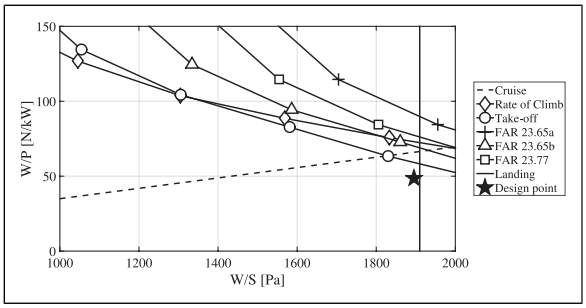

Figure 4. Diagram of constraint for the SkyVultur aircraft.

The design point chosen for the SkyVultur aircraft is lying close to the intersection of the constraint curves, which is generally desirable to reduce both the engine size and wing geometry (see Figure 4). The design point matches a power loading equal to 48.6 N/kW and a wing loading equal to 1.89 kPa. From this design point, the aircraft is characterized by a wing area (S_{ref} = 42.5 m^2). Furthermore, a trade-off study for selecting the engine was carried out. Pratt & Whitney and Honeywell Aerospace companies stand out in the market. After several analyses, the SkyVultur aircraft is equipped with two turboprop PT6A-65SC engines rated 820 kW each one.

Aerodynamic design

The aerodynamic design is required to calculate the aircraft's lift-to-drag (L/D) ratio in several layouts. We used a multi-fidelity approach, starting by a robust low-fidelity solver for rapid and reliable results since the initial design required considerable changes at several iterations. Subsequently, low-fidelity methods were validated against high-fidelity CFD analysis for a specific configuration. Outputs from aerodynamic analysis were used to evaluate the performance characteristics of the SkyVultur aircraft.

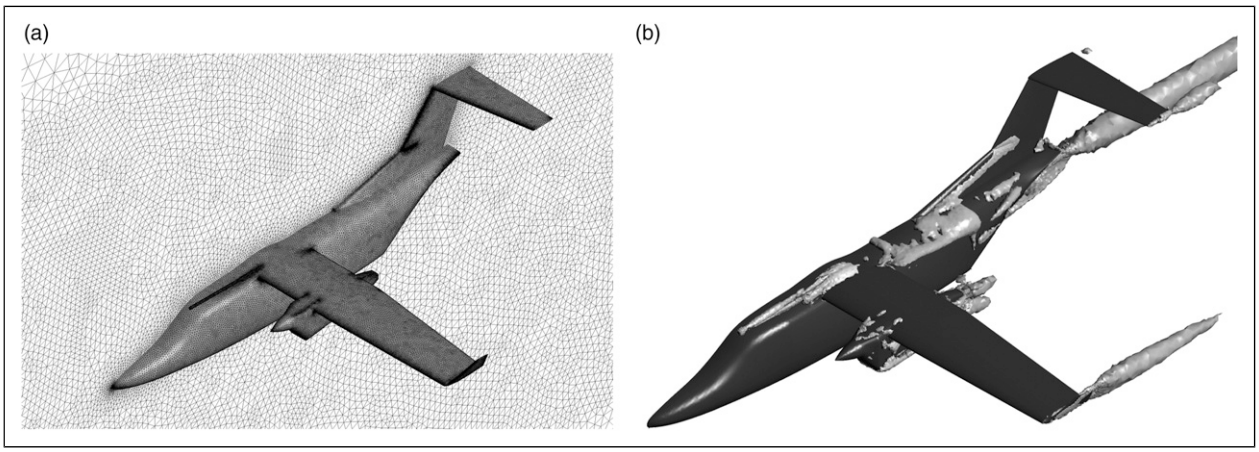

Figure 5. Results of the proposed CFD methodology. (a) SkyVultur surface mesh and (b) vortex core visualization in CFD model (Q-criterion = 0.001 $1/s^2$; $\alpha = 0°$). CFD: computational fluid dynamic.

Low-fidelity solver. The lift characteristics were obtained using an in-house tool, which solves steady aerodynamics using the vortex lattice method (VLM). In sum, the singularity element is the vortex line solution of the incompressible potential flow equation ($V = \nabla\phi$), while the imposed boundary condition is that of non-penetration flow on the surface of the wing panels. The input parameters include taper ratio (λ), aspect ratio (AR), chord, wing area (S_{ref}), sweep angle (Λ), dihedral angle (Γ), and twist. Furthermore, it can be specified with the flight conditions like the angle of attack, the flying Mach, and altitude. Output parameters include lift coefficient (C_L), span efficiency factor (e), induced drag coefficient (C_{Di}), and the lift distribution along the wingspan. Note that induced drag was calculated in a plane located at an infinite distance downstream of the configuration, which is perpendicular to the wake (Trefftz plane).

On the other hand, the drag component was calculated by the sum of pressure drag due to viscous separation (C_{D0}) and induced drag. Pressure drag was obtained using a flat-plate skin friction coefficient, an interference factor, the wetted area, and the component "form factor" of each aerodynamic surface. The wetted area of each aircraft component has been estimated through the analysis of 3D CAD drawings. Miscellaneous drag included the wing air refueling pod, belly fairing, and fuselage–wing root fairing. Furthermore, the power plant system drag was calculated by summing both propeller and diffuser components.

High-fidelity solver. Reynolds-averaged Navier–Stokes (RANS) equations were solved using ANSYS software.[30] The primary objective was to provide more accurate information about the flow field around the entire configuration.

A wide computational domain was designed, avoiding the influence of the wall boundaries on the flow (e.g., friction-less walls and no pressure gradient at outlet). For this simulation, the aircraft's true scale along with actual atmospheric and operational conditions were considered (e.g., velocity inlet = 103 m/s and flight altitude = 7600 m).

Appropriate grids were generated for the SkyVultur aircraft based on a grid independence study in function of the drag coefficient. A nonstructured mesh around the entire external geometry was generated, consisting of about 12×10^6 computational elements for symmetry (half geometry) (see Figure 5(a)). Furthermore, to capture the boundary layer effects with high precision, an inflation regulator with 12 layers of prism was imposed around the geometry according to the total thickness. Thus, the first layer was set at $y_f = 1 \times 10^{-3}$ m from the wall, resulting in a y^+ distribution by about 1.0.

For turbulence modeling, the two-equation $\kappa - \omega$ shear stress transport (SST) model was implemented. This model was selected due to its capability to predict the turbulence effects in higher-order terms. The mathematical formulation of the two-equation model considered for the present study is given by Menter.[31] It should be noted that automatic initial conditions were considered, bearing in mind a second-order advection scheme of precision. The convergence control was set to reach 1500 iterations, with a residual target of 1×10^{-5}.

An example of the CFD results is shown in Figure 5(b). The display of the vortical structure (Q-criterion) around the final configuration showed a clear flow separation on specific parts of the aircraft such as the wing–fuselage and nacelle–wing junctions. Likewise, there is a vortex merging formation at the rear part of the aft ramp door, which is caused by the abrupt variation of the cross-sectional profiles around this region. It was an expected outcome considering the cabin arrangements that the aircraft must keep.

Geometry results

Wing. The wing model was designed in three phases: the airfoil optimization, the main wing sizing, and the wingtip selection. Initially, several airfoils implemented in commuter aircraft and STOL-type aircraft were analyzed using rapid two-dimensional simulations. The selection criteria were the aerodynamic efficiency,

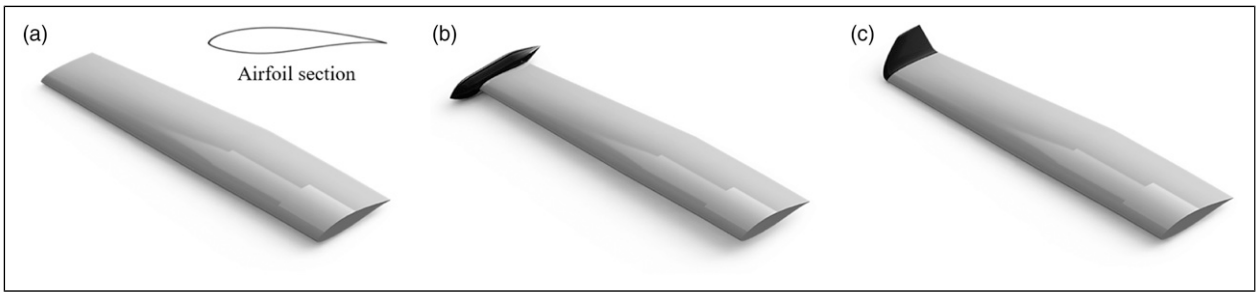

Figure 6. Wing and wingtip configurations. (a) Clean, (b) tip tank, and (c) blended winglet.

maximum lift coefficient, and minimum drag coefficient in order to satisfy the design requirements. Among them, two airfoil sections were considered during the selection process: Do A-5 (used on the Dornier 228 aircraft) and GRUMMAN K-3. The airfoil with the highest aerodynamic efficiency was the GRUMMAN K-3. Then, its coordinates were modified using an optimization method coupling PARSEC parameterization and genetic algorithm based on the technique proposed by Della Vecchia, Daniele, and D'Amato.[32] The airfoil's geometric characteristics were optimized as recommended by the genetic algorithm package until obtaining a series of airfoils with satisfactory characteristics, such as a better aerodynamic efficiency and a higher lift coefficient at stall region. The optimized airfoil is characterized by a maximum thickness of 16% at 31.9% chord and a maximum camber of 2.5% at 67.5% chord. The optimized airfoil can be seen in Figure 6(a).

The main wing was modeled using the aforementioned VLM code. After several iterations by interacting with the static stability module, the wing planform was optimized from a full-tapered wing to a constant chord-tapered outer wing, providing stiffens to the structure and reducing aerodynamic losses at the tips. Some geometric characteristics include washout angle equal to 1.0° from wing root to tip, which helps to reduce induced drag and improve stall characteristics. Furthermore, a dihedral angle equal to −1.0° was imposed for lateral stability reasons, in order to reduce the keel effect, which is caused by the wing position with respect to the fuselage (high wing). Therefore, this angle satisfactorily contributed to the aircraft's maneuverability.

Finally, two wingtip devices (tip tank and blended winglet) were designed in order to evaluate their benefits and maximize the aerodynamic efficiency of the SkyVultur aircraft. Even though the advantages of wingtip devices have been known for decades,[33] there are no reports about wingtip optimization and performance analysis on turboprop military transport aircraft. Such wingtip devices were selected due to their simple certification process because the flight is not critically compromised in case of a failure.

The tip tank (Figure 6(b)) was designed to increase the fuel capacity, reduce induced drag, and improve spin recovery characteristics. Tip tanks extend beyond the lateral edge of the wing and therefore increase the area and AR. The blended winglet (Figure 6(c)) was designed considering a near-vertical extension of the wingtip while keeping a cant angle equal to 45° based on the Whitcomb optimization.[34] It features a smooth chord variation in the transition section, refusing some of the potential induced drag reduction in return for less viscous drag and less need for tailoring the sections locally. It should be noted that the wingtip devices were designed without exceeding the wing loading constraints, according to the design space of the aircraft. Experimental and numerical analysis of such configurations are presented hereafter.

Fuselage. The fuselage of the SkyVultur aircraft was designed to provide adequate accommodation for payload and all aircraft systems, without compromising the safety and comfort of the crew. The length of the fuselage (l_f) was estimated using semi-empirical models of similar aircraft. In this case, turboprop and twin-engine aircraft, considering 0.5 m as a safety margin due to the aft ramp door. Thus, the fuselage length is calculated as a function of the MTOW ($l_f = 0.169 W_o^{0.51} = 17.5$ m).[28]

We defined a fuselage fineness ratio (l/h) by about 8.0, in order to design the cross section of the cabin. This value is very close to that one of major competitors.[29] Figure 7 shows the main design characteristics of the SkyVultur aircraft fuselage. In Figure 7(a), the fuselage design and the possible cabin arrangements are presented. It is observed an easy cabin access thanks to the three different doors and the easy reconfiguration for different possible applications (passengers, cargo, and paratroop).

On the other hand, the cross-sectional profiles and the internal arrangement of the passengers' cabin (section B–B) are depicted in Figure 7(b). The cross sections of the fuselage were planned with a superellipse shape ($|x/a|^n + |y/b|^n = 1$). This formula defines a closed curve contained in the rectangle $-a \le x \le +a$ and $-b \le y \le +b$. The parameters a and b are called the semi-diameters of the curve, and n controls the nature of the cross-sectional corners. In this case, $n = 3$, which allowed a rectangle with rounded corners. This configuration also aids to reduce the wetted area and therefore the parasite drag. Note that the upper side of the cross sections B–B and C–C were not considerably changed because of limitations in changing the structure of the body. However, the lower part of these profiles was modified due to the aft ramp door location. It should be noted that the cross section around the ramp

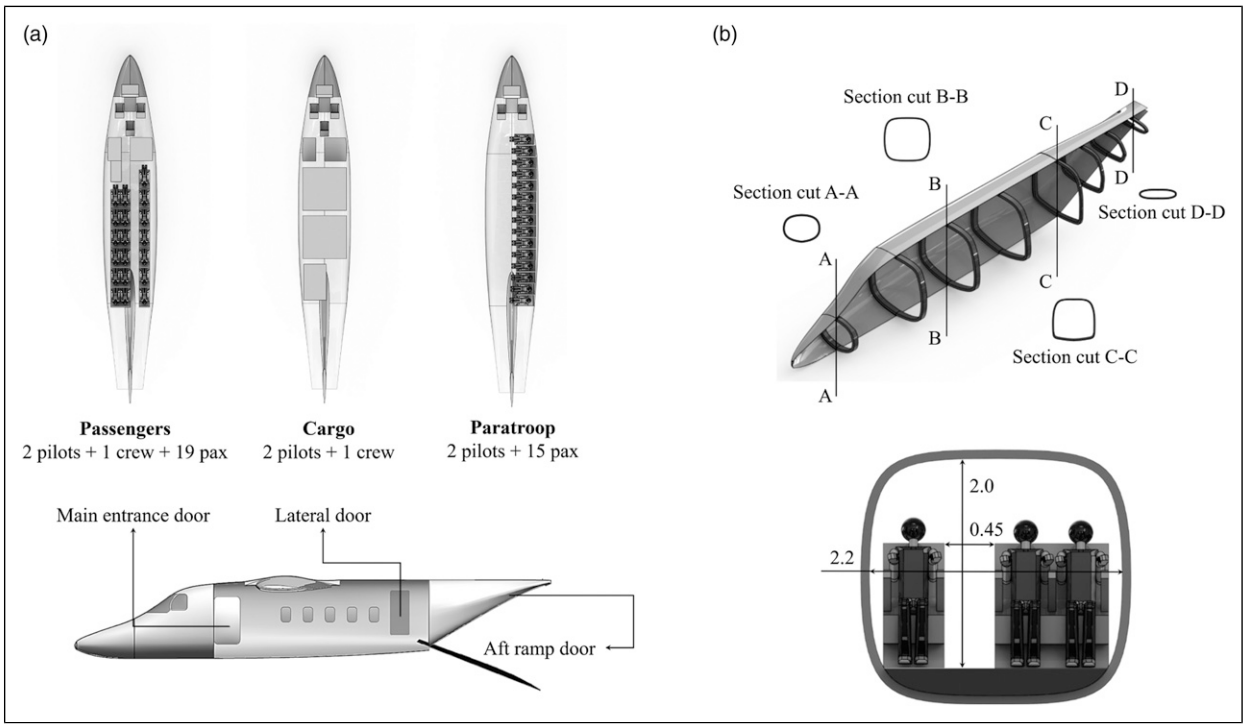

Figure 7. Main design characteristics of the SkyVultur aircraft fuselage. (a) SkyVultur cabin arrangement and design of all possible versions and (b) fuselage cross sections and internal design of passengers' cabin, dimensions in meters.

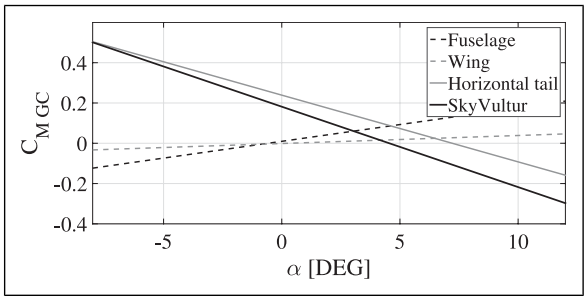

Figure 8. Pitching moment coefficient breakdown.

door region (section D–D) was designed by changing the upsweep angle in order to obtain the least possible drag coefficient.[35]

Tail. Tailplanes were designed to achieve stability and flight quality characteristics. Both vertical and horizontal tails were modeled on the basis of standard values for twin-engine turboprop aircraft. These values were used for calculating the respective tail areas, considering the moment arm obtained from 50% of the fuselage length since the SkyVultur aircraft is using wing-mounted turboprop engines.[28]

The fuel consumption during the entire mission and the launch of cargo or paratroopers can result in a wide range of gravity center (CG) locations. Therefore, the tail must provide sufficient downforce to achieve a balance with the moment generated by the wing, that is, the slope of the pitch moment coefficient must be negative ($(\partial C_M/\partial\alpha) < 0$), for satisfying longitudinal stability criteria. Figure 8 shows the pitching moment contribution of each aerodynamic surface in function of the angle of attack (α). It is observed the wing and fuselage instability contributions (positive slope); however, the overall stability of the aircraft was essentially defined by the horizontal tail. The choice of the horizontal tail airfoil and its angle of incidence (α_i) played an important role in the longitudinal stability analysis since it directly affects the slope of the tail lift curve (NACA 0012, $\alpha_i = -1.0°$). This contribution allowed a static margin of 17% and a neutral point of 35% regarding the location of the mean aerodynamic chord. Such results suggested that the SkyVultur aircraft is stable longitudinally, at least where the impact of the stall is negligible.

Upon evaluating the longitudinal stability of the aircraft, the impact of the main aerodynamic shape parameters on the lateral-directional stability was investigated. Mathematically, the necessary criterion to guarantee the directional static stability is to obtain a positive coefficient of yawing moment due to sideslip ($dC_n/d\beta) > 0$. Likewise, to ensure that the aircraft is laterally stable, the coefficient of rolling moment due to sideslip has to be slightly negative, thus ($dC_l/d\beta) < 0$.

Figure 9 shows typical plots of yawing moment (Figure 9(a)) and rolling moment (Figure 9(b)) against sideslip angle. After iterative calculations, the contribution of the vertical tail on directional stability was carefully estimated, determining the final tail design. Likewise, the contribution of side forces to dihedral effect was assessed to ensure adequate lateral stability of the aircraft. In this

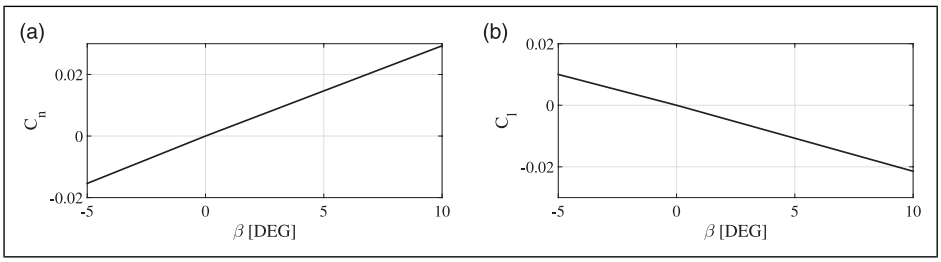

Figure 9. Lateral-directional static stability. (a) Yawing moment coefficient and (b) rolling moment coefficient.

way, both aerodynamic and flight stability requirements are satisfied.

Revised layout. A step-by-step procedure concerning the conceptual design of the SkyVultur aircraft has been addressed in the previous sections. The final concept came from a series of iterations among the design modules. Some additional analyzes included characterizing the available thrust and sizing the control surfaces. In this context, the available thrust was calculated based on blade element and vortex theories. The first theory involved the Prandtl's lifting line to optimize the induced efficiency of the propeller. The second theory was used to calculate the performance of the propeller, based on the thrust and power coefficients varying the pitch angle. Several propellers available in the market were analyzed, highlighting the Hartzell and Avia categories. Among them, the HC-B4 TN-5CL propeller showed maximum efficiency in function of the advance ratio. Thus, this propeller was selected to work on the SkyVultur aircraft with a total of five blades per engine.

Control surfaces (ailerons, elevator, and rudder) were designed in compliance with Sadraey's guidelines.[36] Therefore, extreme flight conditions were considered, guaranteeing control authority around a certain axis in any flight condition. Finally, flaps were designed and mounted at the wing's trailing edge. These are deployed downward to increase the wing's effective curvature, thus increasing the maximum lift coefficient, which in turn reduce both the aircraft's stall speed and takeoff and landing distances. The dimensional drawings and the isometric view of the SkyVultur aircraft are shown in Figure 10.

Experimental setup

Once defined the overall geometry of the SkyVultur aircraft, a high-fidelity analysis on the developed wingtip devices was performed. Only the wing and wingtip sections were analyzed, avoiding the fuselage and tail sections. Several works have followed this strategy to reduce computational and experimental costs.[37–40]

Experimental tests were performed in the blower-type (closed wall test section) wind tunnel of the Department of Aeronautical Engineering, São Carlos School of Engineering-University of São Paulo (see Figure 11). This wind tunnel has an engine that generates 25.5 kW of power, providing a volumetric flow of about 115,000 m^3/h. The dimensions of the test section are 1.05 m × 0.8 m × 2.0 m. The maximum speed is 25 m/s with a turbulence intensity of about ± 0.15%. Additional information about the EESC-USP Experimental Aerodynamics Laboratory can be found in Ref. 41.

Atmospheric conditions were measured using a weather station, which registered the following conditions: static pressure (P = 92.3 kPa), static temperature (T = 23°C), and density (ρ = 1.08 kg/m^3). Airspeed was measured by using a micro manometer which has an uncertainty of ±0.1 Pa and a static-pitot placed in the wind tunnel output section. In addition, to measure the aerodynamic forces exerted on the models, the wind tunnel is equipped with a TE-81 aerodynamic balance (uncertainty ±0.02 N), which is connected by cables to strain gauges for the measurement of lift, drag, and pitching moment. The aerodynamic balance was set to take 5000 samples with a frequency sample of 500 samples per second.

Figure 11 also depicts all the scale models (1:33-scale) installed in the wind tunnel. The mockups were manufactured using the Cliever CL2 pro plus 3D printer, which uses polylactic acid as building material. The models were internally reinforced to withstand the aerodynamic loads associated with the wind tunnel testing. Their surfaces were finished to simulate the skin of a real aircraft. The models were tested at angles of attack ranging from −4° to 20° with 2° increments. A turn-disk was used to set the angle of attack at wind-off and wind-on conditions.

Given the experimental limitations, the Reynolds number of the experimental setup differs from the Reynolds number of the actual flight conditions. In fact, the Reynolds number (based on the mean aerodynamic chord) of the test cases was 2.5 × 10^5, whereas the actual Reynolds number is 12.1 × 10^6. Therefore, trip strips at the wing leading edge (≈5%) of chord were set in order to promote the transition from laminar to turbulent flow. The size of the trip strips was 0.3 mm in height. Wind tunnel wall interference effects were not considered, as the blockage phenomena is less than 8%.[42]

To conclude, RANS simulations coupled to the SST turbulence model were carried out to validate the wind tunnel experiments of each wingtip configuration. In this case, the atmospheric conditions of the experimental setup

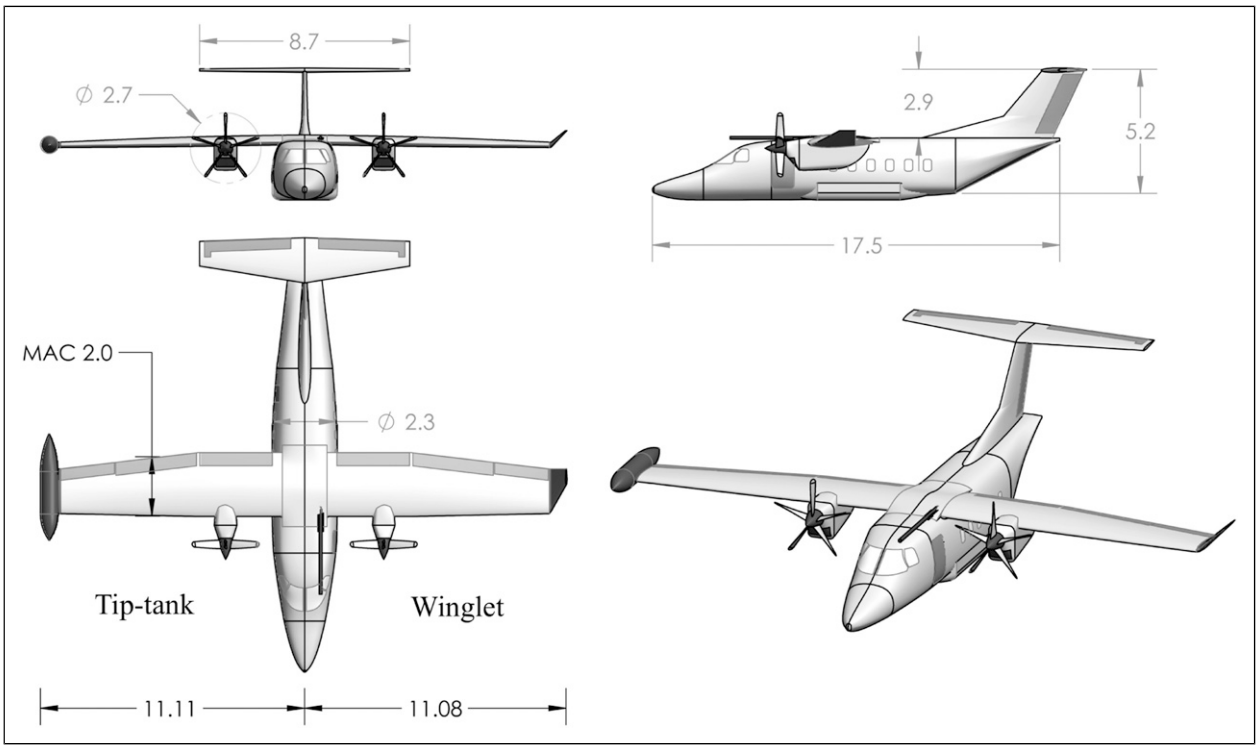

Figure 10. The SkyVultur aircraft geometry at the end of the conceptual design phase (tip tank and blended winglet versions evidenced), dimensions in meters.

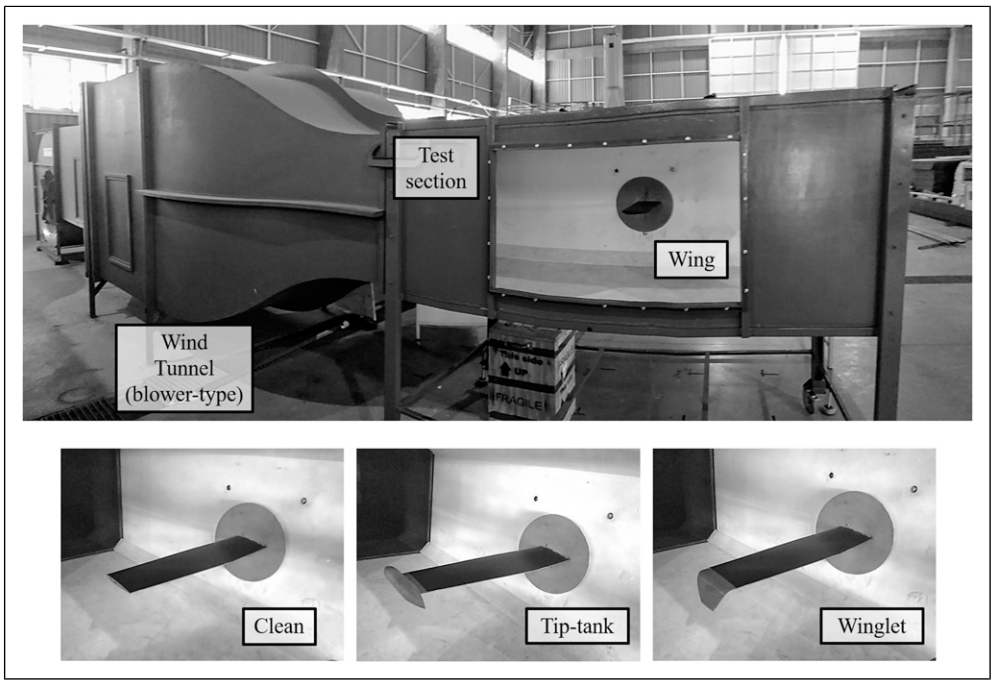

Figure 11. Blower-type wind tunnel at São Carlos Engineering School, University of São Paulo.

were adjusted to the computational setup. Furthermore, the boundary domain was drawn as a virtual box with the same dimensions as the wind tunnel test section, ensuring the models are practically positioned at the same distance from the inlet, as well as avoiding angle corrections for the effective angle of attack.

Results and discussion of configurations

First comparison and validation

In Table 2, a first experimental–numerical comparison about the aerodynamic coefficients of the wing/wingtip analysis is reported. The agreement for lift and moment

Table 2. Experimental and CFD results comparison.

Configuration	Clean			Tip tank			Blended winglet		
Parameter	Exp	CFD	% error	Exp	CFD	% error	Exp	CFD	% error
C_L for zero α	0.51	0.50	1.55	0.47	0.46	2.08	0.52	0.51	1.72
$\partial C_L/\partial\alpha$	0.0709	0.0712	0.42	0.0784	0.0789	0.63	0.0797	0.0802	0.62
C_{Lmax}	$1.36_{@16°}$	$1.42_{@18°}$	4.41	$1.40_{@16°}$	$1.45_{@18°}$	3.57	$1.44_{@16°}$	$1.48_{@18°}$	2.77
C_{D0}	0.0224	0.0211	5.80	0.0251	0.0235	6.37	0.0234	0.0219	6.41
$\partial C_D/\partial C_L^2$	0.0366	0.0355	3.00	0.0201	0.0193	3.98	0.0193	0.0185	4.14
$(L/D)_{max}$	$23.10_{@2°}$	$24.01_{@0°}$	3.93	$24.02_{@4°}$	$24.98_{@2°}$	3.99	$26.77_{@4°}$	$27.71_{@2°}$	3.51
C_M for zero α	−0.0232	−0.0224	3.31	−0.0214	−0.0207	3.27	−0.0181	−0.0175	3.45
$\partial C_{M(GC)}/\partial\alpha$	−0.0189	−0.0192	1.59	−0.0184	−0.0187	1.63	−0.0169	−0.0172	1.78

CFD: computational fluid dynamic.

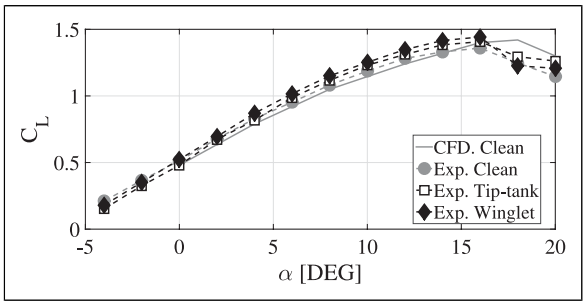

Figure 12. Lift coefficient.

characteristics is fairly adequate, especially at low to moderate angles of attack, where there is still no viscous separation. It is an anticipated outcome since SST turbulence model capability is strong in regions where fluid separation has no major impact.[31] In contrast, a greater dispersion (on the order of 4.0%) at high angles of attack is found due to the higher level of complexity in the flow pattern arising from the stall region, which is more difficult to be numerically simulated.

On the other hand, we noted a significant uncertainty (by about 6.0%) in drag prediction using RANS simulations in comparison with experimental results. Such differences can be attributed to the turbulence modeling and its impossibility to accurately predict transition at low-Reynolds numbers. Despite that result, such variations are acceptable for preliminary design phases.

Since the differences between numerical simulations and experimental analysis lie within the limits of aerospace investigations,[43] the following figures depict the experimental results of all configurations and only the CFD results of the clean configuration for validation purposes. Furthermore, specific flight conditions from the CFD simulations were selected in order to understand the changes in the tip vortex distribution and their effect on the aerodynamic characteristics.

Aerodynamic charts

Lift and drag coefficients. Figure 12 shows the variations of lift coefficients in terms of angle of attack. It is clear from this figure that the slopes of the linear region ($\partial C_L/\partial\alpha$) (near zero degrees angle of attack) are quite similar. However, lift coefficient is substantially increased at all angles of attack with blended winglets. This finding is attributed to the winglet's ability to alter the lift distribution of the wing by altering the tip vortices.

At high angles of attack (i.e., from $\alpha = 8°$ to $\alpha = 16°$), tip tank configuration evidenced a C_L increase by about 2.94% compared to the clean configuration. Meanwhile, the blended winglet presented an overall increase of 5.9%. This finding demonstrated the importance of installing winglet devices on the SkyVultur wing since its benefits would improve efficiency across the entire mission profile.

On the other hand, Figure 13 shows the variations of the drag coefficient among the wingtip configurations. In Figure 13(a), it is represented the drag polar chart. The superiority of the winglet device is evident since it displayed higher lift values at lower drag values than the other configurations, that is, the lift-to-drag ratio is better at almost every angle of attack. This result is easier to understand in Figure 13(b), where the variation of drag coefficient with the square of lift coefficient ($\partial C_D/\partial C_L^2$) is depicted (induced drag parameter). There are two interesting cut points in this figure. The first point is between the winglet and clean curves which occurs at $C_L^2 = 0.33$ and $C_D = 0.024$. This means that from $\alpha = 2°$, the SkyVultur aircraft with winglets would have a higher aerodynamic efficiency than the clean configuration due to reduced induced drag. The second point is between the tip tank and clean curves which occurs at $C_L^2 = 0.55$ and $C_D = 0.031$. It can be seen that the tip tank device has a similar effect than the winglet despite the obvious increase in parasite drag resulting from the addition of wetted area, that is, even though the tip tank presented a higher parasite drag, there is a favorable aerodynamic effect as the lift coefficient increases.

This result is demonstrated by looking at the curl velocity contours extracted from CFD simulations (see Figure 14). In this figure, the generation of vortices in each wingtip configuration can be observed qualitatively. A contour plane was located at 0.7 m downstream from the wall of the models. Two flight conditions were selected in

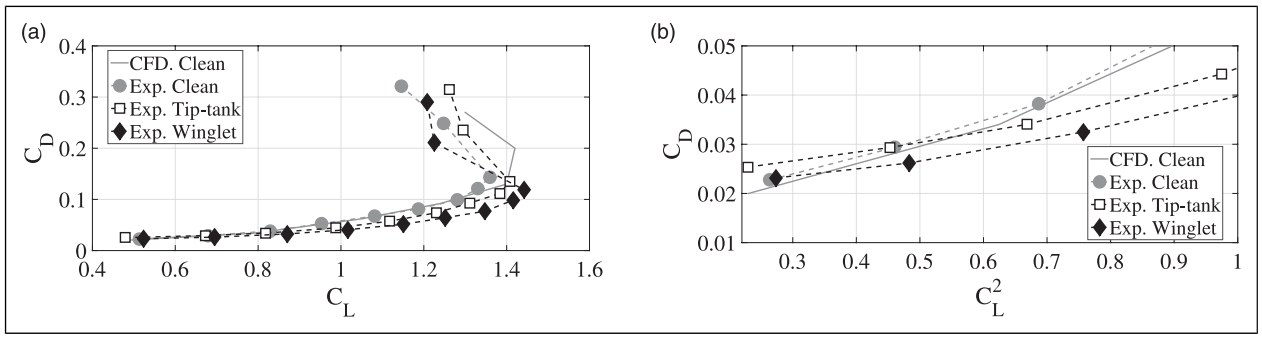

Figure 13. Drag coefficient. (a) Drag polar and (b) induced drag.

terms of lift coefficient. Figures 14(a), (c), and (e) were taken at $C_L = 0.7$, which is the lift coefficient for maximum aerodynamic efficiency. Figures 14(b), (d), and (f) were taken at $C_L = 1.3$, which is a flight condition close to stall. In both conditions, the vortex size from the winglet device is significantly smaller than the other configurations. Therefore, an increase in the effective AR is evident which represents the reduction of the induced drag.

It should be noted that the intensity of the vortices generated by the clean and tip tank configurations are similar at $C_L = 0.7$. This outcome can be confirmed in Figure 13(b), where at $C_L^2 = 0.49$, the clean and tip tank configurations generate an equivalent drag coefficient, $C_D \approx 0.03$. In contrast, the winglet configuration presented a $C_D \approx 0.026$ for the same lift coefficient. Therefore, the visual difference from Figures 14(c)–(e) can be translated into an induced drag decrease of 15%.

Combining the results of flow vortex and aerodynamic performance, the blended winglet configuration obtained the best overall performance regarding reduction in vortex strength downstream of the wing. This behavior is also observed in the aerodynamic efficiency chart given in Figure 15, where a clear superiority of the blended winglet (14.71%) over the clean configuration is observed. While the efficiency improvement given by the blended winglet is obvious, note that all configurations displayed a similar pattern, where the maximum values were obtained between the interval $0.65 \leq C_L \leq 0.85$, which corresponds to $2° \leq \alpha \leq 5°$. Finally, there was a clear agreement between the CFD and experimental methods in the linear region. However, the weakness of the CFD method for predicting viscous drag was evident at high angles of attack due to the predicted separation regions.

Pitching moment coefficient. Figure 16 depicts the variation of the pitching moment coefficient (C_M) in function of the angle of attack. C_M values were taken from a new reference coordinate located at the same percentage of CG location with respect to the model's mean aerodynamic chord. It is found that the CFD clean curve fits with the experimental curve at low angles of attack. However, at high angles of attack, there is a greater difference due to the stall effects. Given the experimental curves, there is no significant differences among curve slopes ($\partial C_{M(GC)}/\partial\alpha$) in the linear portion. However, as the blended winglet configuration increased lift by the reduction of the tip vortex (see Figure 14), the pitching moment of the wing itself is reduced. This proved that wingtip devices restrict the size and formation of wingtip vortices, reducing induced drag and reducing the angle of attack required to produce a certain lift coefficient. The established lift benefits of these specific wingtip devices for the SkyVultur aircraft demonstrated that it is possible to produce increased lift without adversely affecting the aircraft's stability parameters.

Aircraft performance analysis

In the previous section, we presented a detailed aerodynamic evaluation of the SkyVultur's wing, highlighting the benefits of the wingtip devices. In sum, both tip tank and blended winglet presented a significant increase in span efficiency. However, it is clear that the blended winglet is the optimal design since it reduces the intensity and magnitude of the wingtip vortices; while at the same time, it does not produce interference vortices under the flight conditions examined.

The final stage of this investigation was to determine the performance of the SkyVultur aircraft along specific phases of its mission profile. A summary of the aerodynamic performance comparing the baseline concept (full configuration without wingtip devices) and the final concept (full configuration with blended winglet) for actual operating conditions is shown in Table 3. The left-hand side of the table shows the validation scheme of the design methodology, that is, the evaluation of the main aerodynamic characteristics of the aircraft from low-fidelity (VLM) and high-fidelity (CFD) simulations. Parasite drag, induced drag, and aerodynamic efficiency at cruise condition are compared. Note that drag coefficients from high-fidelity methods showed higher values than results from low-fidelity methods. This is an expected outcome since low-fidelity methods cannot exactly predict viscous and interference effects. However, the accuracy of the low-fidelity design method deviated as much as 8.0% from the CFD validation, which is a low-percentage difference, as low-fidelity analysis was only used to

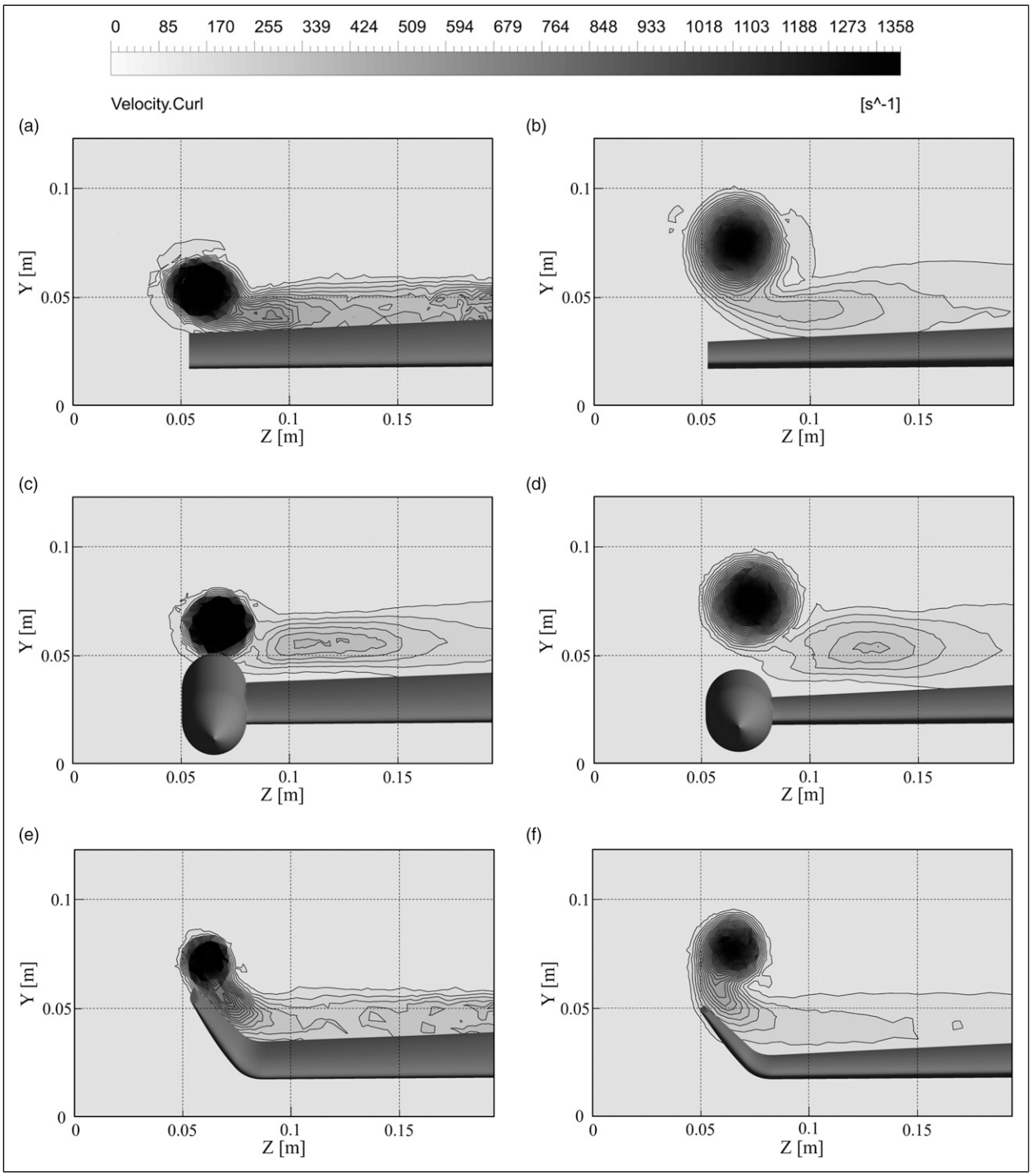

Figure 14. Vorticity contours for the same lift coefficient. Contour plane located at 0.7 m from the wing leading edge. (a) Clean, C_L = 0:7. (b) Clean, C_L = 1:3. (c) Tip tank, C_L = 0:7. (d) Tip tank, C_L = 1:3. (e) Blended winglet, C_L = 0:7. (f) Blended winglet, C_L = 1:3.

obtain rapid estimates of the aerodynamic coefficients during the first steps of the design process.

On the other hand, the right-hand side of the table shows the results from the CFD optimization study. The aerodynamic values were used to evaluate the performance characteristics of the SkyVultur aircraft considering the simple mission profile. Flight dynamics equations based on Eshelby,[44] along with statistical factors that estimate the fuel weight throughout the segments of the aircraft mission, were used to estimate the performance. Since the method requires an estimate of the thrust-specific fuel consumption, values from the available literature were adapted to our performance model. As a result, the blended winglet assembly did not reflect a significant variation in the empty weight, as the difference between the configurations was about 3%. This means that the wing loading was not affected considerably, so the design constraints have been met.

Furthermore, the aerodynamic efficiency of the final concept is considerably high compared to the baseline concept. Therefore, a better match for long range per mission was obtained. This result can be translated into a decrease of cruise fuel consumption of about 5.6% when operating at the maximum available thrust.

Finally, one of the main features of the SkyVultur aircraft is the takeoff field length and the capability to operate on very short runways, considering the accelerate–stop distance as critical item for a twin-engine aircraft. Therefore, takeoff and landing distances were calculated using the acceleration force provided by the propeller, weight, and the sum of the drag and friction drag, as shown in Ref. 28 These forces were calculated at 70% of the takeoff speed, without exceeding 20% of stall speed.[6] Table 3 shows the takeoff and landing distances of the SkyVultur aircraft at medium sea level, including the use of flaps deployed at 40°.

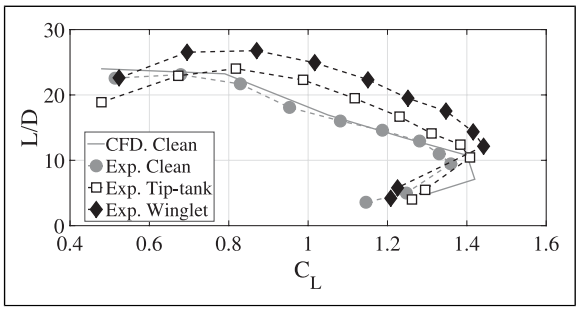

Figure 15. Aerodynamic efficiency.

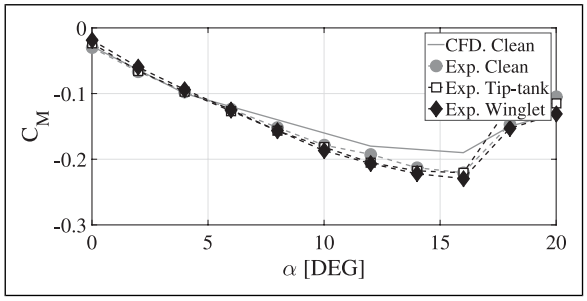

Figure 16. Pitching moment coefficient.

Design validation from databases

In order to verify that the SkyVultur aircraft meet market demands, some performance and geometric comparisons among certified aircraft are presented in Table 4. Due to its multipurpose objective, the SkyVultur aircraft demonstrated a close correlation among design parameters of similar aircraft, as well as desirable characteristics such as higher cruise speed, lower stall speed, STOL distances, and the ability to carry heavy payloads, even operating long distances. The winglet device distinguishes the SkyVultur aircraft from other configurations, allowing to minimize the fuel consumption, by achieving a higher aerodynamic efficiency through higher mission lift coefficients. It should be noted that the SkyVultur aircraft's output data vary depending on the mission to be performed. For example, if the payload is reduced, the overall takeoff weight is reduced as well, allowing for greater operating ranges by using less fuel.

Even though the SkyVultur aircraft was designed to defend the sovereignty of the Colombian airspace, its performance characteristics indicate that other countries might be interested in joining the concept. Finally, we can infer that the aircraft's design space was respected during conceptual design, providing an acceptable level of accuracy for use in the preliminary design stage or for

Table 3. Comparison and validation between the baseline and optimized configuration of the SkyVultur aircraft.

Validation				Computational fluid dynamic optimization			
Parameter	Low-fidelity (baseline)	High-fidelity (baseline)	% difference	Parameter	Baseline concept	Final concept	% difference
C_{D0}	0.0375	0.0406	7.93	Empty weight (kN)	38.25	39.39	2.93
C_{Di}	0.0072	0.0077	6.71	Cruise fuel weight (kN)	7.85	7.43	−5.49
C_L/C_D	8.94	8.28	7.66	Wing surface (m^2)	42.50	43.54	2.47
				Aspect ratio	10.12	11.27	10.75
				L/D	8.28	9.06	9.0
				Cargo range (km)	750	804	7.22
				Maximum range (km)	1450	1560	7.64
				Rate of climb (m/s)	6.65	6.97	4.91
				Takeoff distance (m)	750	720	4.0
				Landing distance (m)	640	614	4.1

Table 4. Design validation through databases (information taken from crosschecks on web-based unclassified data).[45–48]

Parameter	Dornier do 228	PZL M28 Skytruck	CASA C-212 Aviocar	Cessna 408 SkyCourier	SkyVultur
Wingspan (m)	17	22.06	20.28	21.95	22.16
Length (m)	16.56	13.1	16.15	16.71	17.5
Wing surface (m^2)	32	39.72	41	—	43.54
Aspect ratio	9	12.25	10	—	11.27
Empty mass (kg)	3900	4354	3780	—	4015
Takeoff mass (kg)	6400	7500	8000	—	8122
Stall speed (m/s)	41.11	41.11	40.27	—	40.7
Cruise speed (m/s)	87.5	67.77	98.33	102.7	103
Takeoff/landing runs (m)	792/451	548/499	610/462	1006/-	720/614
Cargo range (km)	396	—	835	740	804
Service ceiling (m)	7620	7620	7925	7600	7600
Propulsion system	Turboprop	Turboprop	Turboprop	Turboprop	Turboprop
Wingtip device	Not	Not	Not	Not	Winglet

benchmarking. Therefore, subsequent design phases such as preliminary and detailed studies can be expedited.

Conclusions

A new STOL twin-engine turboprop aircraft has been designed to haul freight or 19 passengers, which is able to perform commuter and tactical transport missions. The general methodology for the conceptual design is first developed by considering traditional methods and in-house algorithms; whereas CFD simulations and wind tunnel experiments aided on the optimization of the main performance characteristics.

Results obtained by these methods have shown fair agreements for practical engineering purposes. For example:

- Wind tunnel tests showed that no substantial improvement in aerodynamic efficiency was found using a tip tank device. However, additional fuel tanks may be mounted at different positions on the airframe to enhance the aircraft's fuel carrying capacity. The most common place could be under the wing using pylons, providing a substantial increase from the point of view of endurance, without any drastic modification to the payload requirements.
- The standout feature of the SkyVultur aircraft was the implementation of an efficient winglet device, which increases the effective AR, reducing the induced drag and improving aircraft performance. This drag reduction also provided fuel efficiency (reducing block fuel burn by about 6%), which reduces emissions and operating costs when compared to similar configurations.
- Although the benefits of wingtip devices for induced drag reduction are well documented in the literature, the net advantage on tactical transport aircraft has never been studied. In this context, the blended winglet provided a considerable improvement in aerodynamic efficiency despite a very small increase in wingspan and wing surface. Thus, the wing primary structure is not changed and the flight qualities do not present a negative impact.
- To our knowledge, the SkyVultur aircraft is the first design proposed in Colombia that includes extensive aerodynamic and performance analyzes. Its performance characteristics enable it to operate in a shared mission, that is, in cooperation with countries that share the same geographic environment and common security problems. Ultimately, the main purpose is to provide profitable and low-cost alternatives.
- Further research will provide structural and dynamic stability analysis in order to assess the aircraft's flying qualities and proof of concept.

Acknowledgements

The authors express their gratitude to those involved in this project, especially to the engineers Dayana López, Eric Rodriguez, Julian Perez, Juan Velandia, Duvan Espejo, Jhosep Rodriguez, Deisy Rojas and Dina Torres for their effort in unique aspects of the designed aircraft. The authors are thankful to the International Cooperation Commission (CCint) and the Oficina de Relaciones Interinstitucionales (ORI) for the student exchange program between the Department of Aeronautical Engineering, São Carlos Engineering School - University of São Paulo and Programa de Ingeniería Aeronáutica, Fundación Universitaria los Libertadores. Special thanks to the jury members of the First Aeronautical Design Contest in honour of the 100th anniversary of the Colombian Air Force (FAC). The authors also thank Dr. Jorge Nisperuza for his assistance in the work team's formation. Special thanks to Professor Dr. Fernando M. Catalano for providing us the facilities of the Experimental Aerodynamics Laboratory (LAE-1).

Declaration of conflicting interests

The author(s) declared no potential conflicts of interest with respect to the research, authorship, and/or publication of this article.

Funding

The author(s) received no financial support for the research, authorship, and/or publication of this article.

ORCID iD

Pedro David Bravo-Mosquera https://orcid.org/0000-0001-5666-9465

References

1. Norton B. *STOL progenitors: the technology path to a large STOL aircraft and the C-17A*. Reston, VA: American Institute of Aeronautics and Astronautics, 2002.
2. Edi P. The development of n-250 military version. *WSEAS Transactions Fluid Mech* 2006; 1(8): 832–837.
3. Menarchik D. *Powerlift–getting to desert storm: strategic transportation and strategy in the new world order*. Westport, CT: Greenwood Publishing Group, 1993.
4. Bravo-Mosquera PD, Cisneros-Insuasti ND, Mosquera-Rivadeneira F, et al. Stem learning based on aircraft design: an interdisciplinary strategy developed to science clubs colombia. *Cienc Poder Aéreo* 2019; 14(1): 204–227.
5. Morán JJD, Reina JJ and Reina RJ. Transporte aéreo estratégico militar en las operaciones militares modernas. *Ciencia y Poder Aéreo (Spanish version)* 2019; 14(1): 114–147.
6. Agency EAS. *Certification specifications for normal, utility, aerobatic, and commuter category aeroplanes-Cs-23*, 2012.
7. Frischtak CR. Learning and technical progress in the commuter aircraft industry: An analysis of Embraer's experience. *Res Pol* 1994; 23(5): 601–612.
8. Williams LJ. *Small transport aircraft technology*. Stanford, CA: Scientific and Technical Information Branch, National Aeronautics and Space, 1983, Vol. 460.
9. Nicolosi F, Della Vecchia P and Corcione S. Design and aerodynamic analysis of a twin-engine commuter aircraft. *Aerosp Sci Technol* 2015; 40: 1–16.
10. Corcione S, Nicolosi F and Della Vecchia P. Wind tunnel tests of a new commuter aircraft. In: 22th AIDAA Conference, Linkoping, September 2013.
11. Nicolosi F, Corcione S and Della Vecchia P. Commuter aircraft aerodynamic characteristics through wind tunnel tests. *Aircraft Eng Aerosp Tech* 2016; 88(4): 523–534.
12. Nicolosi F, De Marco A and Della Vecchia P. Stability, flying qualities and longitudinal parameter estimation of a twin-engine cs-23 certified light aircraft. *Aerosp Sci Technol* 2013; 24(1): 226–240.
13. Nicolosi F, Vecchia PD and Ciliberti D. Aerodynamic interference issues in aircraft directional control. *J Aerosp Eng* 2014; 28(1): 04014048.
14. Nicolosi F, De Marco A and Vecchia PD. Flight tests, performances, and flight certification of a twin-engine light aircraft. *J Aircraft* 2011; 48(1): 177–192.
15. Della Vecchia P and Nicolosi F. Aerodynamic guidelines in the design and optimization of new regional turboprop aircraft. *Aerosp Sci Technol* 2014; 38: 88–104.
16. Lappas I and Ikenaga A. Conceptual design and performance optimization of a tip device for a regional turboprop aircraft. *Aerospace* 2019; 6(10): 107.
17. Bravo-Mosquera PD, Cerón-Muñoz HD, Díaz-Vázquez G, et al. Conceptual design and cfd analysis of a new prototype of agricultural aircraft. *Aerosp Sci Technol* 2018; 80: 156–176.
18. Kaparos PP, Papadopoulos C and Yakinthos K. Conceptual design methodology of a box wing aircraft: a novel commercial airliner. *Proc Inst Mech Eng Part G: J Aerosp Eng* 2018; 232(14): 2651–2662.
19. Hosseini S, Ali Vaziri-Zanjani M and Reza Ovesy H. Conceptual design and analysis of an affordable truss-braced wing regional jet aircraft. *Proc Inst Mech Eng Part G: J Aerosp Eng* 2020. Epub ahead of print. DOI: 10.1177/0954410020923060
20. Bravo-Mosquera PD, Abdalla AM, Cerón-Muñoz HD, et al. Integration assessment of conceptual design and intake aerodynamics of a non-conventional air-to-ground fighter aircraft. *Aerosp Sci Technol* 2019; 86: 497–519.
21. Iwaniuk A and Wiśniowski W. Optimization of small aircraft parameters in the initial phase of the project. *Proc Inst Mech Eng Part G: J Aerospace Eng* 2017; 231(12): 2248–2258.
22. Iwaniuk A and Piwek K. Preliminary design and optimization for fleet to be used in the small air transport system. *Proc Inst Mech Eng Part G: J Aerosp Eng* 2018; 232(14): 2615–2626.
23. Vouvakos X, Kallinderis Y and Menounou P. Preliminary design correlations for twin civil turboprops and comparison with jet aircraft. *Aircraft Eng Aerosp Tech* 2010; 82(2): 126–133.
24. Marinus BG and Poppe J. Data and design models for military turbo-propeller aircraft. *Aerosp Sci Technol* 2015; 41: 63–80.
25. Marinus BG and Maison J. Fuel weight estimates of military turbo-propeller transport aircraft. *Aerosp Sci Technol* 2016; 55: 458–464.
26. Marinus BG and Quodbach L. Data and design models for civil turbopropeller aircraft. *J Aircraft* 2020; 57: 1–16.
27. Roskam J. *Airplane design*. Lawrence, KS: DARcorporation, 1985.
28. Raymer D. *Aircraft design: a conceptual approach*. Reston, VA: American Institute of Aeronautics and Astronautics, Inc., 2018.
29. Torenbeek E. *Synthesis of subsonic airplane design: an introduction to the preliminary design of subsonic general aviation and transport aircraft, with emphasis on layout, aerodynamic design, propulsion and performance*. New York: Springer Science & Business Media, 2013.
30. ANSYS Fluent. *Ansys fluent theory guide*. USA: ANSYS Inc, 2011, Vol. 15317, pp. 724–746.
31. Menter FR. Two-equation eddy-viscosity turbulence models for engineering applications. *AIAA J* 1994; 32(8): 1598–1605.
32. Della Vecchia P, Daniele E and D'Amato E. An airfoil shape optimization technique coupling parsec parameterization and evolutionary algorithm. *Aerosp Sci Technol* 2014; 32(1): 103–110.
33. Merryisha S and Rajendran P. Review of winglets on tip vortex, drag and airfoil geometry. *J Adv Res Fluid Mech Therm Sci* 2019; 63(2): 218–237.
34. Whitcomb RT. *A design approach and selected wind tunnel results at high subsonic speeds for wing-tip mounted winglets*. Washington, DC: NASA Lang-ley Research Center, 1976.
35. Mirzaei M, Karimi MH and Vaziri MA. An investigation of a tactical cargo aircraft aft body drag reduction based on cfd analysis and wind tunnel tests. *Aerosp Sci Technol* 2012; 23(1): 263–269.
36. Sadraey MH. *Aircraft design: a systems engineering approach*. New Hampshire: John Wiley & Sons, 2012.
37. Cerón-Muñoz HD and Catalano FM. Experimental analysis of the aerodynamic characteristics adaptive of multi-winglets. *Proc Inst Mech Eng Part G: J Aerosp Eng* 2006; 220(3): 209–215.
38. Wei Z and Meijian S. Design optimization of aerodynamic shapes of a wing and its winglet using modified quantum-behaved particle swarm optimization algorithm. *Proc Inst Mech Eng Part G: J Aerospace Eng* 2014; 228(9): 1638–1647.

39. Zhang G, Peyada N, Go TH, et al. Design and investigation of a bio-inspired ventilated flapping wing. *Proc Inst Mech Eng Part G: J Aerosp Eng* 2015; 229(4): 747–763.
40. Siddiqi Z and Lee J. A computational fluid dynamics investigation of subsonic wing designs for unmanned aerial vehicle application. *Proc Inst Mech Eng Part G: J Aerosp Eng* 2019; 233(15): 5543–5552.
41. Catalano F. The new closed circuit wind tunnel of the aircraft laboratory of university of sao paulo, brazil. In: 24th international congress of the aeronautical sciencies ICAS, Yokohama, September 2004.
42. Sorensen JN, Shen WZ and Mikkelsen R. Wall correction model for wind tunnels with open test section. *AIAA J* 2006; 44(8): 1890–1894.
43. Mavriplis DJ, Vassberg JC, Tinoco EN, et al. Grid quality and resolution issues from the drag prediction workshop series. *J Aircraft* 2009; 46(3): 935–950.
44. Eshelby M. *Aircraft performance: theory and practice*. Reston, VA: American Institute of Aeronautics and Astronautics, Inc., 2000.
45. Dornier-228. A platform you can rely on. https://dornier228.ruag.com/en (2021, accessed 14 April 2021).
46. PZL-M28-Skytruck. M28 virtual tour. https://m28aircraft.com/ (2021, accessed 14 April 2021).
47. CASA-C-212-Aviocar. Multi-purpose transport aircraft. http://www.flugzeuginfo.net/acdata_php/acdata_c212_en.php (2021, accessed 14 April 2021).
48. Cessna-408. Cessna skycourier. https://cessna.txtav.com/en/turboprop/skycourier (2021, accessed in 14 April 2021).